International Journal of Biological Macromolecules 330 (2025) 148078

Contents lists available at ScienceDirect

International Journal of Biological Macromolecules

journal homepage: www.elsevier.com/locate/ijbiomac

Molecular and functional characterization of the retinitis pigmentosa G90V mutation in a conformationally stabilized rhodopsin background

Pol Fernandez-Gonzalez [a], Sylwia Jencz [b], Steven O. Smith [c], Philip J. Reeves [b], Pere Garriga [a,*]

[a] Grup de Biotecnologia Molecular i Industrial, Centre de Biotecnologia Molecular, Departament d'Enginyeria Quimica, Universitat Politècnica de Catalunya-Barcelona Tech, Edifici Gaia, Rambla de Sant Nebridi 22, 08222, Terrassa, Catalonia, Spain
[b] School of Life Sciences, University of Essex, Colchester, CO4 3SQ, United Kingdom
[c] Department of Biochemistry and Cell Biology, Stony Brook University, Stony Brook, NY, USA

ARTICLE INFO

Keywords:
Rhodopsin
Phototransduction
Protein stability
Retinal degeneration

ABSTRACT

Mutations in the photoreceptor protein rhodopsin can lead to visual dysfunction and retinal degeneration. The G90$^{2.57}$V mutation, in the second transmembrane helix, causes a retinitis pigmentosa phenotype. A conformationally stabilized wild-type rhodopsin bearing an engineered disulfide bond (N2C/D282C) was developed for structural studies of disease-associated mutations. However, this extra disulfide bond may mask the native conformational features of rhodopsin mutants. Here, we investigate the structural and functional consequences of the G90$^{2.57}$V mutation in this stabilized context. The G90$^{2.57}$V substitution disrupts interactions within the retinal binding pocket, particularly with E113$^{3.28}$ in transmembrane helix 3, which stabilizes the Schiff base linkage to 11-*cis*-retinal. Our results demonstrate that the N2C/D282C disulfide bond counteracts the destabilizing effects of the G90$^{2.57}$V mutation by enhancing thermal and chemical stability of the pigment and improving chromophore regeneration. These findings underscore the importance helix and loop interactions in rhodopsin function and highlight the potential of structural modifications to rescue impaired mutants. Furthermore, our work provides novel insights into the effect of engineered disulfide bonds on the structure and dynamics of rhodopsin mutants associated with retinal diseases and allows one to dissect the effects of the disulfide bond from those of the rhodopsin mutation alone.

1. Introduction

Rhodopsin (Rho) plays a crucial role in mediating vision under dim-light conditions [1,2]. As a model visual receptor, the structural and functional dynamics and properties of Rho have been extensively examined due to their significance in the visual phototransduction process. Moreover, Rho is one of the best characterized receptors in the large G-protein-coupled receptor (GPCR) superfamily. As a representative GPCR, Rho has served as an important model system for elucidating GPCR activation mechanisms.

In its dark-adapted state, Rho consists of a polypeptide known as opsin, covalently bound to the vitamin A aldehyde derivative, 11-*cis*-retinal (11CR), through a protonated Schiff base (SB) linkage to K296$^{7.43}$ [3,4] (superscript refers to the general numbering system for GPCRs [5]) in transmembrane (TM) helix 7 of the protein. This chromophore acts as an inverse agonist thus preventing activation of the photoreceptor in the dark [6]. Binding of rod opsin to 11CR to form Rho takes place in the rod outer segments discs [7], where the retinal is delivered from the retinal pigment epithelium.

Mutations in the gene encoding Rho (*RHO*) have been associated with several retinopathies over the years [8–10]. Retinitis pigmentosa (RP) is a group of retinal degenerative diseases affecting more than 1.5 million patients worldwide [11] characterized by photoreceptor cell degeneration that causes impaired day and night vision and can eventually lead to blindness [12]. Over 150 mutations associated with RP have been found in the RHO gene over the years, most of them being point mutations inherited as an autosomal dominant trait [8]. Depending on the position and the residue change, mutations can exert different effects on the protein; some mutants can fold normally and reach the cell surface whereas others have reduced expression levels, abnormal

Abbreviations: 11CR, 11-*cis*-retinal; DM, n-dodecyl-β-D-maltoside; DTT, dithiothreitol; GPCR, G-protein-coupled receptor; Gt, transducin; PMSF, phenylmethylsulfonyl fluoride; *RHO*, gene encoding rhodopsin; Rho, rhodopsin; RP, retinitis pigmentosa; SB, Schiff base; TM, transmembrane; WT, wild-type.

* Corresponding author at: Departament d'Enginyeria Quimica, Universitat Politècnica de Catalunya-Barcelona Tech, Spain.
E-mail address: pere.garriga@upc.edu (P. Garriga).

https://doi.org/10.1016/j.ijbiomac.2025.148078
Received 28 May 2025; Received in revised form 24 September 2025; Accepted 1 October 2025
Available online 4 October 2025

trafficking and are not able to form pigment. Since different mutations can lead to different phenotypes, they have been classified into different classes depending on the mutational effects they exert [8,9]. However, despite detailed knowledge on Rho structure and function of wild-type (WT) Rho, the molecular origin of RP in many of the mutants has been difficult to establish due to their impaired stability. Ongoing efforts aim to further enhance stability to facilitate structural studies and to reach a deeper comprehension on how disease-causing mutations affect the receptor.

Pharmacological rescue of opsin has been previously studied and there is evidence demonstrating that it is able to restore pigment formation in some RP mutants [13,14]. A strategy employed to enhance Rho stability involves engineering an additional disulfide bond (N2C/D282C) at the extracellular domain of the protein, which supplements the native bond between $C110^{3.25}$ and C187. This approach has demonstrated a substantial stabilization effect compared to the WT protein enabling more detailed structural and functional studies of Rho [14–16]. This enhanced stability provides us an excellent candidate for Rho structural and biochemical studies, opening a wide range of opportunities for the potential characterization of different mutations as well as for the study of the opsin interaction with several compounds that may mitigate the impact of mutational changes.

Our study focuses on characterizing both the WT Rho and the $G90^{2.57}V$ mutant in the presence of this additional disulfide bond. The $G90^{2.57}V$ mutant has been widely studied and is particularly interesting because it is associated with RP, specifically it is classified as a mutation causing conformational instability rather than protein misfolding [17]. The reported mutation occurs at $G90^{2.57}$ of the protein, located at the TM2 and oriented toward the interior of the helical bundle (Fig. 1A). Since the engineered protein with the extracellular additional disulfide bond has increased stability, it is widely used for structural studies. We have carried out functional and biochemical characterization of both the WT and the $G90^{2.57}V$ mutant in this stabilized background (WTs-s and $G90^{2.57}$Vs-s) in order to compare them with these proteins previously characterized without the additional disulfide bond [17]. This has allowed insight and a deeper understanding as to how the extra disulfide bond affects the conformational properties of the protein. This study may give us a promising model for the study of different mutations and the visual pathologies associated with them.

Overall, we find that the N2C/D282C disulfide bond can improve the conformational stability of $G90^{2.57}V$ Rho and also its chromophore regeneration without affecting the downstream signal transduction process. This study highlights the advantage of the disulfide-stabilized variants for structural studies, but also the limitations due to the imposed increased stability that is absent in the native protein. This stabilization effect can mask the actual properties of naturally-occurring mutations in Rho associated with retinal disorders. This information can prove to be useful for the development of novel therapeutic approaches that may help counteract the detrimental mutational effects.

2. Materials and methods

2.1. Construction of stable HEK-293S cell lines for tetracycline-induced opsin gene expression, cell culture and protein expression induction

Stable HEK-293S cell lines for tetracycline-induced opsin gene expression (WTs-s and $G90^{2.57}$Vs-s mutant) construction was performed using a modified version of a method previously reported [18] but in this case the gene encoding for both opsins contained a N2C/D282C modification which leads to an extra disulfide bond between position C2 and C282 [14]. HEK-293S cells were grown and maintained in DMEM Ham's F-12 medium supplemented with 10 % (*v*/v) FBS, 2 mM L-glutamine, 100 μg/ml streptomycin and 100 units/ml penicillin. Cells were then grown in an incubator at 37 °C under a 5 % CO_2 atmosphere. Upon approximately 90 % confluence, the DMEM medium was exchanged for fresh medium and 24 h following the addition of the fresh medium protein expression was induced with 5 mM sodium butyrate and 4 mg/l tetracycline for a further 48 h.

2.2. Immunoaffinity purification of expressed opsins

HEK293S cells were harvested 72 h after induction followed by

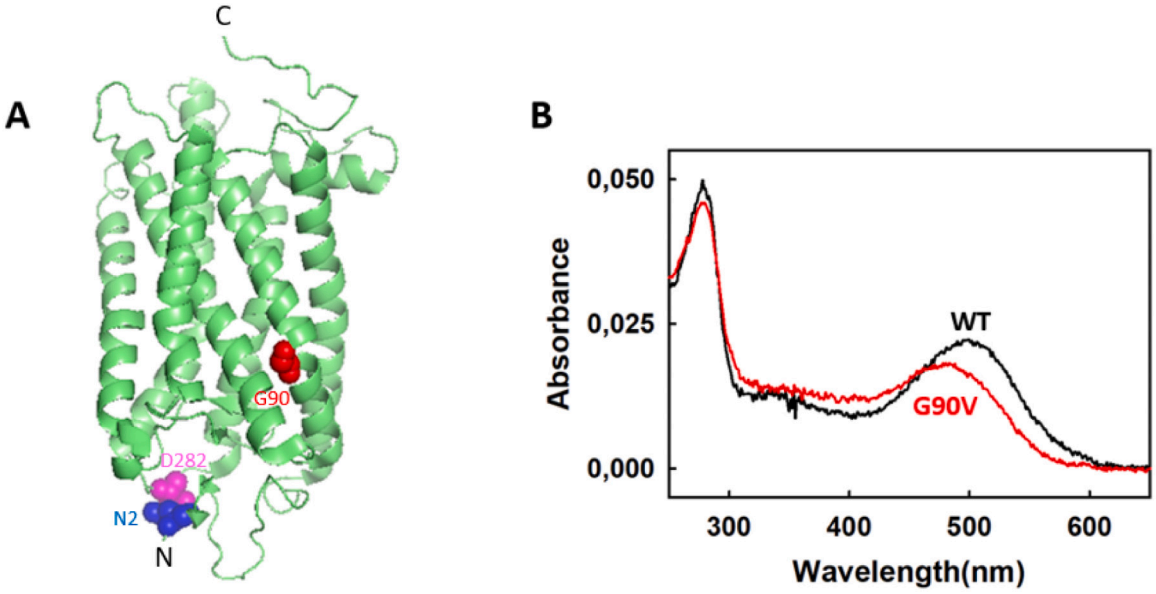

Fig. 1. Structure of Rho with $G90^{2.57}$ position highlighted and representative UV–vis absorption spectra from the first elution of the immunopurified WTs-s and $G90^{2.57}$Vs-s* mutant proteins both regenerated with 11CR. (A) Three-dimensional structure of Rho with residue $G90^{2.57}$ highlighted in red. The amino acids N2 and D282, sites of the N2C/D282C amino acid substitutions that allow formation of the engineered disulfide bond, are indicated in blue (N2) and magenta (D282). The C-terminus (C) and N-terminus (N) of the protein are also depicted for better clarity. The 3D structure was retrieved from the Protein Data Bank (PDB ID: 1U19) and visualized using PyMOL (Schrodinger, LLC. The PyMOL Molecular Graphics System, Version 3.1) (B) Spectra of the pigments recorded immediately after the purification process, WTs-s (*black*) and $G90^{2.57}$Vs-s (*red*). The pigments are in PBS pH 7.4 and 0.05 % DM. All spectra were recorded at a temperature of 20 °C. *For simplicity and to avoid overcrowding, the labels "WT" and "G90V" in all figures refer to the disulfide-stabilized variants WTs-s and G90Vs-s, respectively.

centrifugation at 4000 rpm at 4 °C for 15 min. The pellet was then washed three times with PBS 1× pH 7.4 and centrifuged once more as described. Opsins were subsequently treated in PBS 1× pH 7.4 with a final concentration of 15 μM 11CR by nutating overnight at 4 °C. After pigment regeneration, samples were solubilized by adding a final concentration of 1 % n-dodecyl-β-D-maltoside (DM) and 100 μM phenylmethylsulfonyl fluoride (PMSF) to the mixture and nutating at 4 °C for 1 h. Following solubilization, the lysate was clarified by centrifuging at 15,000 rpm for 30 min at 4 °C. The supernatant was then incubated for 3 h at 4 °C with (CN-Br)-activated sepharose 4B beads coupled to mAb rho-1D4 antibody (purchased from Cell Essentials, Boston, USA) in order to immunopurify WTs-s and G90$^{2.57}$Vs-s mutant Rho. Beads were then washed three times with PBS 1× pH 7.4 containing 0.05 % DM at 4 °C and Rho was eluted by incubating with the same buffer containing 100 μM 9-mer peptide (TETSQVAPA). Rho concentration was then determined by UV–visible spectroscopy, measuring the visible peak absorbance at 500 nm for the WTs-s and 490 nm for the G90$^{2.57}$Vs-s mutant. Upon and after 11CR addition, the steps were performed in the dark or under dim-red light conditions.

2.3. UV–visible absorbance spectral characterization

UV–visible measurements were conducted using a Cary 100Bio spectrophotometer (Varian, Australia) equipped with water-jacketed cuvette holders linked to a circulating water bath. Temperature was regulated by means of a Peltier accessory connected to the spectrophotometer. A final concentration of 0.5 μM of each Rho was used to carry out the assays and this was calculated by using a molar extinction coefficient (ε) of 40,600 $M^{-1} \cdot cm^{-1}$ at 499 ± 1 for the WTs-s and 36,000 $M^{-1} \cdot cm^{-1}$ at 489 ± 1 for the G90$^{2.57}$Vs-s mutant [17]. All spectra were recorded from 250 nm to 650 nm with a bandwidth of 2 nm, a scan speed of 400 nm/min and a response time of 0.5 s.

2.4. Photobleaching and acidification of purified Rho pigments

UV–visible absorption spectra were recorded under dark conditions and subsequently illuminated for 90 s as previously reported [19]. This exposure period was selected to achieve complete photoconversion of the protein samples. Following illumination, the sample was acidified to pH 2.0 to achieve Schiff base reprotonation as previously described [19].

2.5. Thermal bleaching assay

While 37 °C may be a more physiologically-relevant temperature for carrying these experiments, we conducted them at two different temperatures, 48 °C and 55 °C. The purpose of using temperatures above the physiological one is to accelerate the process and simplify the analysis. Thermal decay kinetics were monitored as previously reported by tracking absorbance reduction at the visible maximum over time at specified temperatures [19]. When incorporating dithiothreitol (DTT) treatments, samples were pre-incubated with 1 mM DTT for 30 min at room temperature (20 °C) prior to initiating thermal stability measurements. Half-life values for thermal decay profiles were obtained through curve-fitting analysis of the experimental datasets using either single-exponential models or linear regression approaches in Sigma Plot version 12.5 (Systat Software, Chicago).

2.6. Chemical stability assay with hydroxylamine to measure SB sensitivity

Dark-adapted samples were treated with a final concentration of 50 mM hydroxylamine hydrochloride pH 7 at 20 °C, as previously reported [17]. Absorption spectra were acquired at 2 min intervals (instead of 5 min) for 70 cycles with a 400 nm/min scan rate. Chemical stability was assessed by monitoring absorbance reduction at the visible maximum and retinal oxime formation at 360 nm.

2.7. Rho regeneration with 11CR

Pigment regeneration was performed as previously described [17]. Briefly, a 2.5-fold molar excess of free 11CR in ethanol was added to dark-adapted samples with thorough mixing. After 90 s illumination with a cut-off filter (λ > 495 nm), absorption spectra were collected at 2 min intervals with a 400 nm/min scan rate at 20 °C until visible absorbance reached plateau. Initial reaction rates were determined through single-exponential curve fitting of the experimental datasets using Sigma Plot version 12.5 (Systat Software, Chicago).

2.8. Meta II decay (retinal release) measurements

Retinal release experiments were conducted using a QuantaMaster 4 spectrofluorometer fitted with a TLC50 cuvette holder and Peltier temperature control system as previously described [19] except that the samples were illuminated for 90 s. Half-life values for retinal dissociation kinetics were calculated by applying single-exponential curve fitting to the fluorescence enhancement data using Sigma Plot version 12.5 (Systat Software, Chicago).

2.9. Gt activation assay

Gt activation was measured according to an established procedure [19]. Briefly, 50 nM of dark-adapted Rho was mixed with 500 nM Gt and 5 μM GTP-γ-S at 20 °C until a stable baseline was achieved. Next, the protein mixture was illuminated for 90 s with a 150-watt Dolan-Jenner MI-150, λ > 495 nm filter and the fluorescence increase was monitored. Gt activation was measured at 285 nm excitation with 0.5 nm slit and 338 nm emission with 10 nm slit. Spectra were collected every second (5 consecutive cycles with 25 s intervals) until a plateau was attained. Obtained data from Gt activation assay was fit to a single-exponential function for further analysis using Sigma Plot version 12.5 (Systat Software, Chicago).

3. Results

3.1. UV–visible spectrophotometry of immunopurified proteins

The WTs-s and G90$^{2.57}$Vs-s mutant proteins were immunopurified and the UV–vis spectra were measured right after isolation from 250 nm to 650 nm (Fig. 1B). The UV–vis spectra of the mutant G90$^{2.57}$Vs-s shows a blued-shifted visible absorption band at 488 nm in comparison to the WTs-s protein. The intensity of the chromophoric band for the mutant is also somewhat reduced compared to that of the WTs-s. This lower visible intensity can be attributed to a reduced molar extinction coefficient in the case of the mutant (see a comparison of the spectroscopic data for those Rho's in Table 1). These spectroscopic features are very similar to those of the WT and G90$^{2.57}$Vpreviously characterized [17] indicating that the introduction of the engineered disulfide bond did not noticeably alter the conformation of the proteins and their light-absorbing properties in their ground state (Table 1).

3.2. Photobleaching and acidification

The UV–visible spectra of WTs-s and G90$^{2.57}$Vs-s mutant were measured under dark conditions, after illumination for 90 s and after acidification (Fig. 2). Here, the WTs-s protein showed the expected photobleaching pattern with a shift of the visible band to 380 nm whereas the pattern for G90$^{2.57}$Vs-s was abnormal and quantitatively different from that reported for G90$^{2.57}$V [17]. For G90$^{2.57}$Vs-s, only ≈ 50 % of the 488 nm absorbing species observed before illumination was photoconverted to the 380 nm absorbing species, reflecting an alteration in the photobleaching pathway (Fig. 2B). This behavior was observed in

Table 1
Spectroscopic properties of N2C-D282C WT and G90$^{2.57}$V mutant Rho regenerated with 11CR in comparison with recombinant WT and G90$^{2.57}$V without the extra disulfide bond.

Rhodopsin	λ_{max} (nm)[b]	$A_{280}/A\lambda_{max}$[c]	Thermal bleaching $t_{1/2}$[d] (min)		NH_2OH reactivity $t_{1/2}$[e] (min)
			48 °C	55 °C	
WT[a]	499 ± 1	2.2 ± 0.1	133.4 ± 1.3	/	155.0 ± 10.0
G90V[a]	489 ± 1	3.4 ± 0.2	3.8 ± 0.7	/	3.3 ± 0.7
WTs-s	499 ± 1	2.1 ± 0.1	545.3 ± 0.3	204.8 ± 0.23	274.1 ± 0.5
G90Vs-s	488 ± 2	3.4 ± 0.2	83.6 ± 0.4	6.78 ± 2.14	11.8 ± 1.0

[a] Values for these conditions were taken from a previous study [16].
[b] Mean value and S.D. of the visible peak of samples obtained in independent purifications ($n = 3$) of WT and G90$^{2.57}$V Rho.
[c] These ratios provide an idea of both sample purity and the ability of opsin to form pigment with the chromophore. Data are mean ± S.D. values of independently purified proteins (n = 3).
[d] Thermal bleaching ($t_{1/2}$) of samples. Values are the mean ± S.D. (n = 3) of the time course decay of the visible peak absorbance (λ_{max}) normalized to that of WT rhodopsin. Data points were obtained by using the equation, $\Delta A = (A - A_f)/(A_0 - A_f)$, where A is the absorbance recorded at λ_{max}, A_f is the absorbance at the final time, and A_0 is the absorbance at time 0, and were fit to a single exponential decay function (G90$^{2.57}$Vs-s) or a linear function (WTs-s).
[e] SB stability as determined by the rate constants of hydroxylamine reactivity of the dark state pigments at 20 °C. Values (mean ± S.D., n = 3) were determined by monitoring the rate of λ_{max} absorbance decrease after the addition of hydroxylamine to the samples and adjusted to an exponential rise function with either a single component or a linear function.

the case of the G90$^{2.57}$V [17] but in that case the effect was less pronounced indicating that the presence of the engineered disulfide bond enhanced the kinetics changes in the life-time of the photointermediates. Additionally, acidification of the photoactivated receptors showed an abnormal, and previously not reported, behavior (Fig. 2, blue lines). Typically, upon acidification, illuminated Rho and G90$^{2.57}$V mutant completely shift to ≈ 440 nm [13]. For the S—S stabilized proteins, however, a different behavior is observed where in both, the WT and the mutant visible bands shift first to ≈ 470 nm, and after some time (5 min), this band definitely shifts to 440 nm corresponding to acid-trapped denatured opsin [13].

Additionally, as expected, the difference spectra between the dark and illuminated states for WTs-s (Fig. 2C), indicates a clear spectral shift corresponding to the formation of the Meta II conformation. In contrast, the G90$^{2.57}$Vs-s mutant shows a difference spectrum of lower intensity (Fig. 2D). This reduced amplitude indicates that a smaller fraction of the protein reaches the fully active Meta II conformation upon illumination and that the protein conformation might partially be trapped in a protonated SB photointermediate before reaching the active Meta II conformation.

3.3. Thermal stability in the dark

The thermal stability of the chromophores in the dark was measured by following the decrease in the λ_{max} over time at two different temperatures, 48 °C and 55 °C (Fig. 3). These two temperatures were selected based on previous reports [17] but in this case, thermal stability of the G90$^{2.57}$Vs-s mutant at 48 °C showed an increased stability when compared to that of the G90$^{2.57}$V mutant with only the native disulfide bond. For this reason and due to the slow thermal decay, stability was also studied at 55 °C.

The thermal stability measurements at the temperature of 55 °C show a faster decay for both the WTs-s and the G90$^{2.57}$Vs-s mutant, with the mutant completely decaying after approximately 50 min. Furthermore, when comparing with the stability of both the WT and the G90$^{2.57}$V mutant (without the additional disulfide bond) at 48 °C we observe a significant increase in stability. However, the only protein to

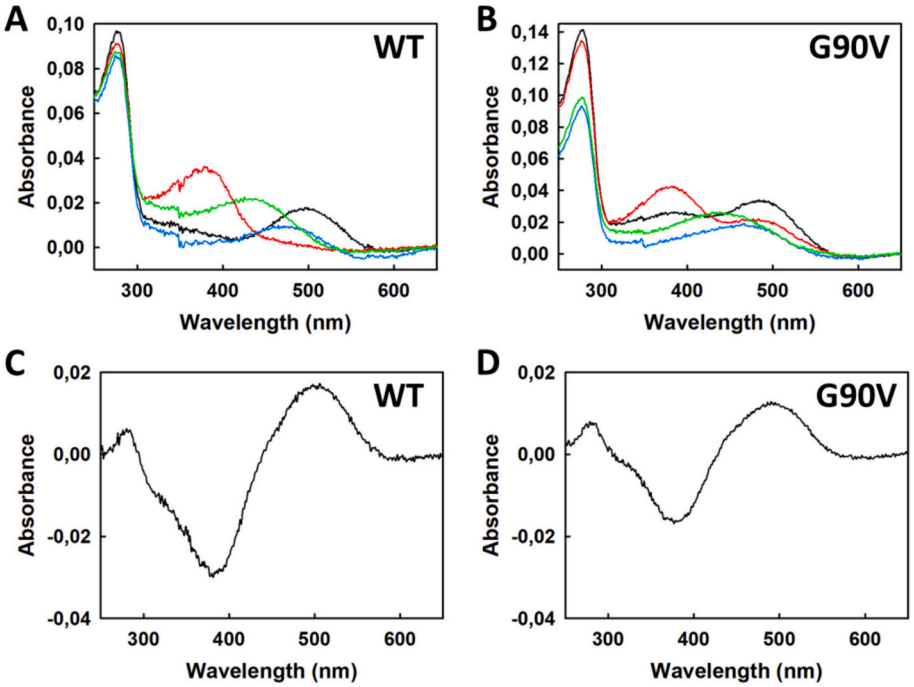

Fig. 2. UV–visible characterization of the immunopurified WTs-s and G90$^{2.57}$Vs-s mutant pigment. UV–visible spectra of WTs-s (A) and G90$^{2.57}$Vs-s (B) regenerated with 11CR. Opsin expression was induced in HEK-293 cells with tetracycline-induced opsin gene expression and pigments were subsequently regenerated and immunopurified with the specific 1D4 antibody. Dark spectra were first recorded (*black lines*), followed by illumination (*red lines*) for 90 s and acidification (*blue lines*) represent spectra right after acidification; green line in panel A and B represent spectra 5 min after acidification. Difference spectra curves of WTs-s (C) and G90$^{2.57}$V (D) were calculated by subtracting the spectrum recorded before illumination from those recorded after the illumination period.

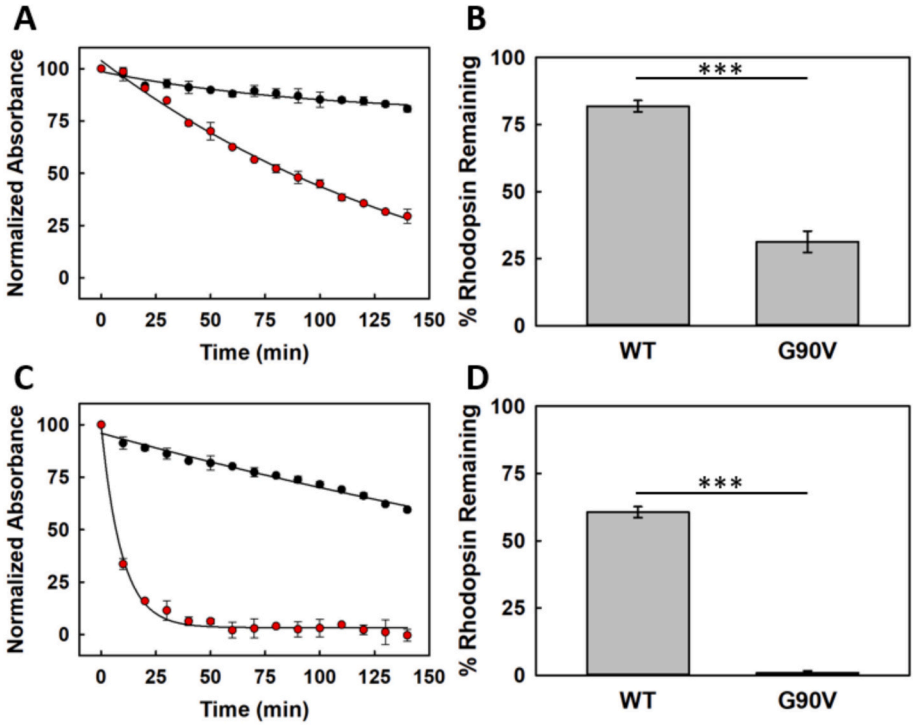

Fig. 3. Thermal stability of the immunopurified WTs-s and G90$^{2.57}$Vs-s mutant at different temperatures. Thermal stability decay of the λ_{max} (499 nm for WTs-s and 488 nm for G90$^{2.57}$Vs-s) of the WTs-s (*black dots*) and G90$^{2.57}$Vs-s mutant (*red dots*) at two different temperatures 48 °C (A) and 55 °C (C), the plots show the decrease of absorbance at the initial λ_{max} in the visible region over 140 min. Also, the percentage of dark-adapted Rho remaining after the 140 min is shown for the two temperatures, 48 °C (B) and 55 °C (D). Mean and standard error of mean values were derived from independent repeated experiments ($n = 3$, $p < 0.001$).

fully decay, in the time course of the experiment, is the G90$^{2.57}$Vs-s mutant at 55 °C and with a $t_{1/2}$ of 6.78 ± 2.14 min. Finally, a quantitative analysis of the remaining dark-adapted Rho was performed by analyzing the final chromophoric band. For the WTs-s pigment at 48 °C, 81.9 ± 2.1 % remained at the end of the experiment, whereas at 55 °C only 60.6 ± 2.0 % was left at the end. On the other hand, for the G90$^{2.57}$Vs-s mutant at 48 °C, 31.3 ± 3.9 % was left being this much higher than the pigment left at 55 °C, where all the dark-adapted pigment was essentially lost (data shown in Fig. 3D).

It was of interest to evaluate the impact of a reducing agent, specifically DTT, on the thermal stability of WTs-s and G90$^{2.57}$Vs-s mutant Rho's. For these experiments, both proteins were incubated with 1 mM DTT for 30 min prior to the thermal stability measurements at 48 °C and 55 °C. The addition of DTT led to a notable reduction in the thermal stability for both proteins when compared to the samples without DTT (compare Figs. 3 and 4). As expected, the results show faster decay at a temperature of 55 °C, where the mutant exhibits a $t_{1/2}$ of 1.3 ± 2.0 min. In contrast, the $t_{1/2}$ of the mutant at 48 °C was 4.5 ± 1.2 min. The WTs-s exhibited similar trends but very different behavior compared to G90$^{2.57}$Vs-s with and without DTT. With the addition of DTT, there is a complete decay of the protein at 55 °C with a $t_{1/2}$ of 9.1 ± 1.8 min. However, at 48 °C the protein did not completely decay and 68.7 ± 1.4 % of the WTs-s remained; $t_{1/2}$ in this case was of 272.0 ± 0.3 min.

3.4. Chemical stability in the presence of hydroxylamine

The reactivity against hydroxylamine was determined in the dark-state in order to measure the SB stability of the pigments (Fig. 5). The SB in dark-adapted WTs-s is known to be highly stable when in the presence of hydroxylamine; however, upon illumination the pigment rapidly reacts with the compound. Mutations in some amino acid residues can lead to a decrease in the stability of dark-state Rho in the

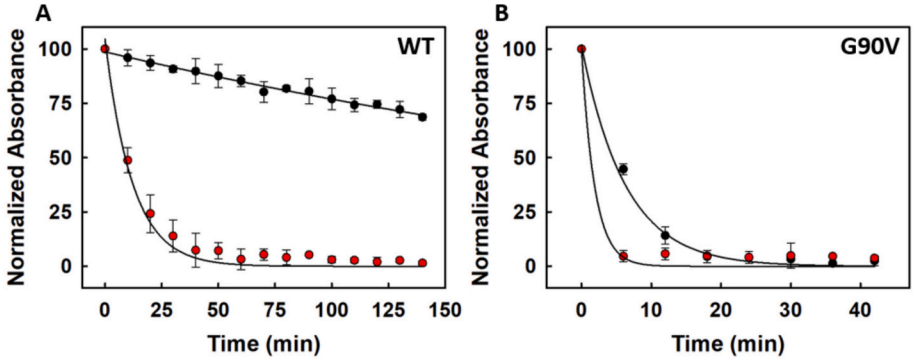

Fig. 4. Thermal stability of the immunopurified WTs-s and G90$^{2.57}$Vs-s mutant at different temperatures and with 1 mM DTT. Thermal stability decay of the λ_{max} (499 nm for WT and 488 nm for G90$^{2.57}$V) of the WTs-s (A) and G90$^{2.57}$Vs-s mutant (B) at two different temperatures 48 °C (*black dots*) and 55 °C (*red dots*), the plots show the decrease of absorbance at the initial λ_{max} in the visible region over 140 min for the WTs-s and 45 min for the mutant.

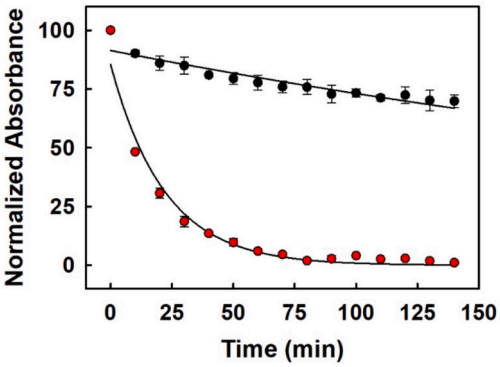

Fig. 5. Chemical stability of immunopurified WTs-s and G90$^{2.57}$Vs-s mutant pigments. The chemical stability of the immunopurified proteins (WTs-s *black dots*; G90$^{2.57}$Vs-s *red dots*) was determined by measuring samples at 20 °C containing a final concentration of 50 mM hydroxylamine during 140 min. The decrease of the Abs at the visible λ_{max} over time was monitored in the dark in the presence of the chemical reagent.

presence of hydroxylamine by affecting the SB environment. This behavior would reflect increased SB accessibility in a more open protein conformation around the SB linkage.

WTs-s behaved as expected and did not show any noticeable change upon the addition of hydroxylamine in the dark. In contrast, G90$^{2.57}$Vs-s mutant showed a high reactivity upon hydroxylamine addition in the dark suggesting a less compact structural configuration of the mutant within the SB environment. Furthermore, when comparing the decay of the mutant with previously published assays using recombinant G90$^{2.57}$V without the extra disulfide bond [13], we can also observe an increased resistance to the effect of hydroxylamine in the dark (Table 1).

3.5. Chromophore regeneration with 11CR

Rho is activated by light and goes through a series of photo-intermediates leading to free opsin before regenerating to its original Rho form by binding to a fresh 11CR molecule [20]. In the presence of some mutations, the ability of Rho to regenerate can be affected leading to a persistent activation of Gt that can damage rod cells and eventually lead to retinal degeneration [21,22].

Here, G90$^{2.57}$Vs-s exhibited a significantly lower regeneration rate when compared to the WTs-s as reported in the initial rate (Fig. 6) indicating a reduced ability of the mutant to regenerate with exogenous 11CR, despite this value being higher than the previously reported for the native mutant [13]. Additionally, both proteins were able to regenerate up to 100 % after illumination indicating that after photobleaching both opsins are still quite stable and have the ability to fully regenerate in presence of an excess of exogenous 11CR.

3.6. Meta II stability for WT and G90$^{2.57}$V pigments

Fluorescence spectroscopy was used to determine the stability of the active state of purified WTs-s and G90$^{2.57}$Vs-s. In the dark-adapted state, the fluorescence of W265$^{6.48}$ residue is suppressed due to quenching by the β-ionone ring of the retinal [23,24]. Upon illumination, retinal is released from the Rho binding pocket thus leading to an increase in W265$^{6.48}$ fluorescence emission, which closely parallels Meta II decay under the given experimental conditions.

The Meta II decay process was slower for the G90$^{2.57}$Vs-s than for the WTs-s as expected, with a significantly higher $t_{1/2}$ (Fig. 7). In both cases, photobleaching of the sample was performed 30 min after the fluorescence signal was stable and samples were illuminated for 90 s. G90$^{2.57}$V mutant showed a high difference compared to the WT with $t_{1/2}$ of 26.8 ± 1.3 min and 13.4 ± 1.2 min, respectively, which is twice as slow. In the case of the pigments without the disulfide bond modification, the observed $t_{1/2}$ was slower for both the WT and the mutant; however, in the latter case, the $t_{1/2}$ value of G90$^{2.57}$V was somewhat slower being 36 ± 1.1 min [13].

3.7. Gt activation assay

During the phototransduction process, the light-activated state of Rho binds and activates Gt in the cytoplasmic face of rod cells [25]. This process conveys the light stimuli to downstream signaling molecules, eventually converting it into a nerve impulse that is processed by the brain. To compare the differences between Gt activation of the WT and the mutant, the process was measured by means of fluorescence spectroscopy. Upon activation of Rho by light, this photoreceptor undergoes a conformational change and binds and activates the G protein Gt thereby altering its local environment resulting in a measurable fluorescence change. The reaction kinetics were analyzed by fitting the fluorescence increase to a single-exponential function, from which the $t_{1/2}$ values were derived.

We find that the G90$^{2.57}$Vs-s mutant exhibits a slight lower ability to activate Gt compared to the WT (Fig. 8 A) with the signal reaching a plateau at a lower fluorescence intensity. Notably, the $t_{1/2}$ shows a significant difference, with a $t_{1/2}$ of 35.3 ± 2.5 min for the mutant

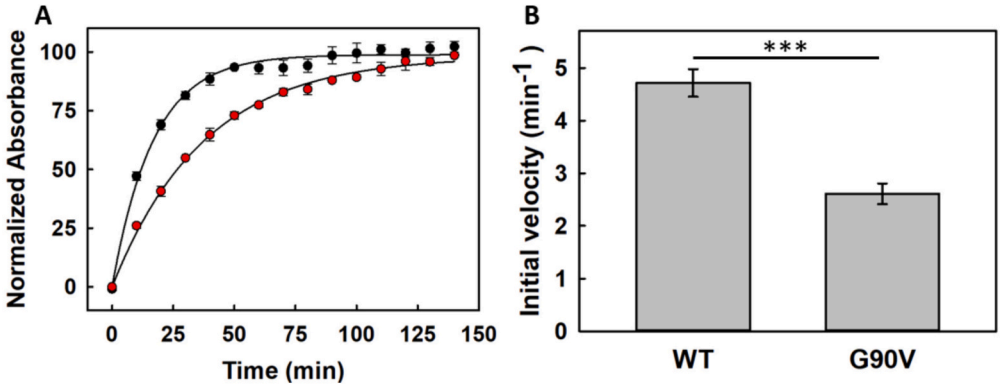

Fig. 6. Chromophore regeneration rates of immunopurified WTs-s and G90$^{2.57}$Vs-s opsins. A 2.5-fold molar excess of 11CR was added to immunopurified WTs-s and G90$^{2.57}$Vs-s mutant pigments. The experiments were conducted in PBS pH 7.4, containing 0.05 % DM. In order to exclude photobleaching of free retinal, samples were illuminated with light of λ > 495 nm. Successive spectra were recorded in the dark at 20 °C until no further increase in λ_{max} was observed. (A) Normalized absorbance values at the visible λ_{max} plotted as a function of time (WTs-s *black dots*; G90$^{2.57}$Vs-s *red dots*), data were fitted to a single exponential function and initial rates derived. (B) Initial rates of chromophore regeneration of WTs-s and G90$^{2.57}$Vs-s. Mean value and standard error were obtained from independent repeated experiments ($n = 3$, $p < 0.001$).

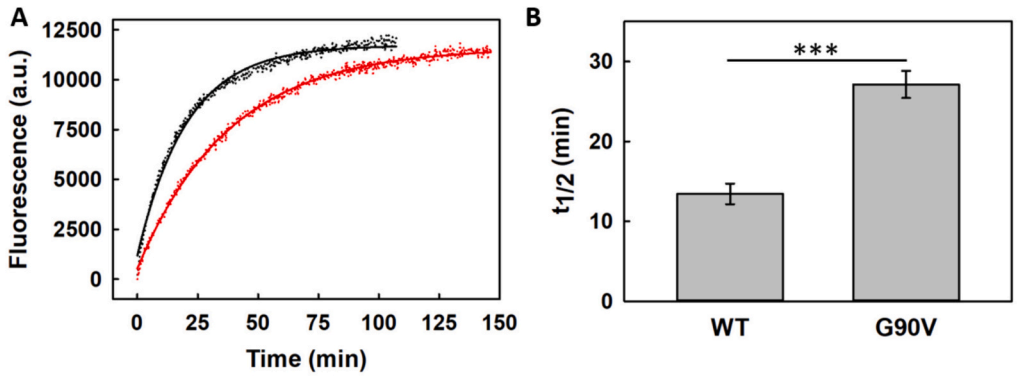

Fig. 7. Meta II decay of the purified WTs-s and G90$^{2.57}$Vs-s mutant both regenerated with 11CR. Samples were incubated at a constant temperature of 20 °C, and after a stable baseline was obtained, samples were photobleached. (A) W265$^{6.48}$ fluorescence signal was tracked over time for WTs-s (*black dots*) and G90$^{2.57}$Vs-s mutant (*red dots*), changes were fitted to a single exponential function. Fits are shown overlayed with raw data, WTs-s fit is shown as a *black line* and G90$^{2.57}$Vs-s fit as a *red line*. (B) Increase in fluorescence intensity data modeled by using a single exponential function was used to determine the $t_{1/2}$. Mean and standard error of mean values were derived from independent repeated experiments (n = 3, $p < 0.001$).

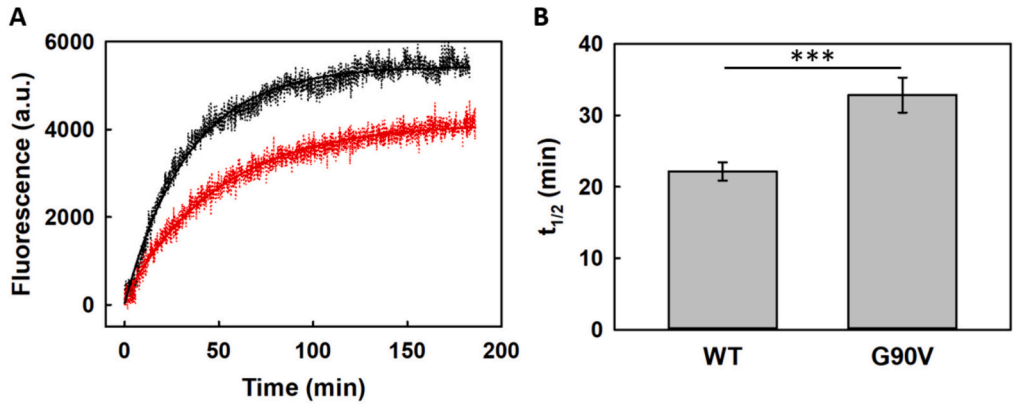

Fig. 8. Gt activation kinetics of the purified WTs-s and G90$^{2.57}$Vs-s mutant both regenerated with 11CR. (A) Gt activation measurement by means of fluorescence spectroscopy for the WTs-s (*black dots*) and G90$^{2.57}$Vs-s (*red dots*) and fluorescence changes at 338 nm were plotted and fitted to a single exponential function. Fits are shown overlayed with raw data, WTs-s fit is shown as a *black line* and G90$^{2.57}$Vs-s fit as a *red line*. (B) $t_{1/2}$ were derived from fitted curves and mean and standard error of mean values were derived from independent repeated experiments (n = 3, $p < 0.001$).

compared to 22.5 ± 1.3 min for the WT (Fig. 8 B).

4. Discussion

Rho belongs to the GPCRs superfamily, a large and diverse family of membrane proteins that play critical roles in a wide range of cellular signaling processes [26]. The involvement of these receptors in numerous physiological processes makes them key targets for pharmaceutical development, with a significant portion of drugs targeting them [27,28]. Among GPCRs, Rho has been often used as a model system for these receptors due to its well-characterized structure and function since it was the first GPCR whose crystal structure was solved at an atomic resolution [29].

The G90$^{2.57}$V mutation, located in the TM2 region of the protein, is linked to RP, a progressive retinal degenerative disease. The G90$^{2.57}$V mutation significantly decreases the conformational stability of the protein rather than promoting protein misfolding [13,17]. There is a need to find suitable strategies to restore the native stability of the receptor as a means to ameliorate retinal degeneration associated with the mutation. One such approach consists of engineering a disulfide bridge (C2-C282) to enhance the stability of Rho. In the case of the G90$^{2.57}$V mutation, this introduced modification has been beneficial for facilitating structural studies, including crystallographic analysis [15]. However, the non-native additional stability imposed by the engineered double bond can mask the actual physicochemical properties of the mutant and hamper the development of novel therapeutic approaches in RP.

Our results clearly show that N2C/D282C mutation notably increases the conformational stability of the WT, particularly that of the G90$^{2.57}$V mutant compared with previous studies with the native proteins [13,17] (see Table 1).

UV–Vis profiles reveal a higher A_{280}/A_{max} ratio for the G90$^{2.57}$Vs-s compared to the WTs-s, although this is likely due to a decreased molar extinction coefficient in the case of the mutant protein [17]. The substitution of Gly in TM helix 2 affects the stability of the protein around the SB linkage by interfering with the native electrostatic interactions with neighboring amino acids and a water molecule [17].

The photobleaching pattern for WTs-s is the same as that for WT but the G90$^{2.57}$Vs-s mutant shows a more prominent remaining band at around 490 nm after illumination when compared to G90$^{2.57}$V [17], which also presents this band. This suggests that not all of the mutant protein undergoes a complete transition to its active Meta II conformational state, possibly due to a shift in the metarhodopsin conformational equilibria. This result would reflect the partial accumulation of a protonated SB photointermediate, possibly Meta I, indicating that the G90$^{2.57}$V mutation alters the photocycle dynamics [17], and this effect appears to be enhanced in the presence of the C2-C282 disulfide bridge. This observation is interesting because it was previously found that RP mutations in the N-terminus display WT bleaching in the C2-C282 background but not in WT background [14], suggesting that the

disulfide bridge may selectively influence the photocycle dynamics depending on the mutation involved. The lower intensity of the G90$^{2.57}$Vs-s difference spectrum further supports the idea that a fraction of the protein remains in an intermediate state after illumination, prior to the formation of the active Meta II conformation. Although this observation is consistent with an altered photocycle, the difference spectra alone does not allow us to unambiguously confirm that the specific intermediate formed is Meta I. At the structural level, the presence of the additional disulfide bond, at the extracellular side of the receptor, may restrict the conformational flexibility needed for the full conversion to the active Meta II photointermediate. The effect of the C2-C282 disulfide bond may exacerbate the effect of the mutation and result in trapping of photointermediates prior to Meta II formation, e.g. Meta I. This possible accumulation of photointeremdiates may also account for the changes in functionality observed in the Gt functional activation by photoactivated rhodopsin in the G90$^{2.57}$Vs-s rhodopsin.

Further discrepancies are observed during acidification with sulfuric acid. Typically, acidification leads to a rapid shift in the A_{max} to ≈ 440 nm, as a result of SB re-protonation [30]. However, in this case, an initial shift to ≈ 470 nm of the visible band is observed right after acidification before eventually setting at ≈ 440 nm after a few min. This delay suggests that the acidification process in these stabilized protein variants involves the transient stabilization of an intermediate state of Rho before reaching the fully denatured re-protonated state, specifically a Meta III-like conformation, potentially due to the increased stability conferred by the disulfide bond.

For the dark-state thermal stability analysis, experiments were conducted at both 48 and 55 °C as previously stated. Results obtained for the mutant at 48 °C are consistent with previous findings on N-terminus RP mutants [14]. At 55 °C, differences became much more evident. The WT protein maintained its structural integrity considerably longer than the mutant, which decayed with a significantly faster kinetic profile. The double bond produced a 4-fold increase in the $t_{1/2}$ for the thermal stability assay for the WTs-s compared to WT [17] whereas, G90$^{2.57}$Vs-s mutant showed about 22-fold increase in stability compared to G90$^{2.57}$V [17] (see Table 1 for comparison of the decay half-life times). It should be noted that the temperatures used to follow the thermal stability of the proteins, 48 and 55 °C, were selected in order to be able to compare our results with those previously reported for the G90$^{2.57}$V mutant [17]. In addition, the thermal decay process for the WTs-s and the G90$^{2.57}$Vs-s mutants is very slow at 37 °C. Therefore, the thermal assay temperatures were selected based on experimental practical reasons but it is obvious that the temperature of 37 °C would have been a more physiologically relevant temperature for this assay. We believe that the key finding regarding protein thermal stability, obtained from the data at the tested temperatures, can be extended to 37 °C, thereby giving the measurements clinical relevance.

We have shown that DTT treatment of WTs-s and G90$^{2.57}$Vs-s revert the thermal stability to values remarkably close to those of the proteins without the extra disulfide bond [17]. In the case of the WTs-s, the percentage of protein remaining after the assay with DTT closely matches that of the WT without the engineered disulfide bond, indicating that the native stability of the protein is unaffected by the reducing conditions once the extra disulfide bond is reduced. This finding also suggests that the native C110$^{3.25}$-C187 disulfide bond is not reduced. In the case of the G90$^{2.57}$Vs-s mutant, the $t_{1/2}$ at 48 °C is almost the same to that previously reported for the mutant with only the native disulfide bond. These results strongly suggests that DTT cleaves the engineered disulfide bridge, leaving only the native C110$^{3.25}$-C187 bond intact. Given that the additional disulfide was introduced to reinforce the structural integrity of Rho, particularly by stabilizing TM2 and TM7 interactions and maintaining the ECL2 conformation, its reduction explains the observed thermal destabilization, as observed previously [14].

Additionally, the G90$^{2.57}$Vs-s mutant exhibited significantly reduced chemical stability while in the presence of hydroxylamine in the dark when compared to the WTs-s which might be a feature of the mutation affecting the SB environment. Here, G90$^{2.57}$Vs-s showed 3.5-fold increase in the $t_{1/2}$ compared to G90$^{2.57}$V for hydroxylamine reactivity, whereas WTs-s showed a 1.8-fold increase in reactivity compared to the WT. The modified interaction between the counterion and the chromophore (PSB) might increase the susceptibility of the SB to solvent exposure and hydroxylamine reactivity in the dark. Consequently, considering that mutations in G90$^{2.57}$V of Rho can still bind 11CR and are capable of producing functional pigments, the instability of the mutant protein is likely due to the enhanced accessibility of the SB linkage to hydroxylamine in the dark state reflecting a less compact structure at its local environment. In contrast the Meta II stability, measured by fluorescence spectroscopy, appears to be unaffected by the newly introduced disulfide bond.

Regarding the regeneration capacity of the protein, we report here that WTs-s Rho exhibits a regeneration efficiency comparable to that of the WT without the extra disulfide bond, which suggests that the introduction of the disulfide bond does not interfere with the structural rearrangements required for 11CR re-binding. In contrast, the G90$^{2.57}$V mutant shows improved regeneration capacity compared to its counterpart lacking the disulfide bond [17] which underscores the stabilizing effect of the N2C/D282C on the structural integrity of the mutant at the opsin state where the regeneration with the chromophore has to take place. This also indicates that the new version of the disulfide stabilized mutant can partially mitigate the structural disruptions introduced by the mutation, particularly in the SB environment and the TM2-TM3 interface.

Upon light activation, Rho binds Gt and this leads to a conformational change in the Gα subunit that enables its binding to GTP with subsequent GDP release. Upon binding to GTP Gα dissociates from Rho and the Gβγ subunit and this process is capable of regulating the signal transduction cascade by interacting with several downstream effectors [25,31]. It is because of the dissociation of Gα from the Gβγ subunit that fluorescence previously quenched can be detected thus being able to monitor Gt activation by Rho [19]. We find a normal behavior for Gt activation from the WTs-s, while for G90$^{2.57}$Vs-s the plateau of the fluorescence signal related to Gt activation is reached at a lower fluorescence signal. Furthermore, the activation of Gt by G90$^{2.57}$Vs-s has a significantly slower kinetics than that of WTs-s. We suggest that this phenomenon could be linked to the altered photobleaching pattern observed for the G90$^{2.57}$Vs-s mutant. The reduced conformational stability and the altered Gt activation kinetics, as a result of the steric and electrical changes at the core of the retinal binding pocket, can be underlying causes of the malfunction of this mutated protein leading to the RP phenotype.

Studies of Rho mutations over the years have concluded that misfolding is usually based on low pigment yield [14], intracellular accumulation [32], altered glycosylation patterns [33] or non-native disulfide bonds [34]. However, no defects on folding kinetics or stability were reported. Nevertheless, over the years, different Rho mutants exhibit decreased thermal stability, suggesting that it might be a common property of a neglected subset of mutations leading to RP. This is the case of the G90$^{2.57}$V mutation in Rho where the replacement with Val may cause steric hindrance and hydrophobic effects in the vicinity of the SB linkage, thus altering optimal helix packing and leading to structural reorganization that may propagate through the TM domain and into the intra and extracellular environments.

A particularly critical aspect of G90$^{2.57}$V mutation lies in its effect on the retinal binding pocket and the chemical environment surrounding E113$^{3.28}$, with an important water molecule in the vicinity. This residue located in TM3, close to the protonated SB, is the primary counterion neutralizing this positive charge [35] with one of the largest values of free energy binding in Rho. This fact indicates that this is a functionally important water molecule involved in the deprotonation step of the SB at the Meta II state. That is why the lack of the water molecule can alter the transition to Meta II and also decrease dark state stability. The

structural perturbations caused by the mutation also may partially disrupt packing of TM2 with TM3, destabilizing the interaction between E113$^{3.28}$ and the SB. Furthermore, the altered flexibility of TM2 affects positioning of extracellular loop (ECL) 1 and ECL2, which play roles in facilitating chromophore binding and release. These changes result in a destabilized binding pocket, photobleaching alterations, and slowed-down chromophore regeneration, as observed experimentally.

Although Rho has been proposed to form dimers or higher-order oligomers within the membrane [36,37], the G90$^{2.57}$ residue is situated within TM2 and oriented toward the interior of the helical bundle, where it contributes to stabilizing the retinal binding pocket. Given its inward orientation and separation from established dimerization interfaces, the G90$^{2.57}$V mutation is unlikely to directly interfere with intermolecular interactions required for oligomerization. Therefore, the structural and functional effects reported in this study are expected to result primarily from local alterations within the monomeric unit, rather than from changes in dimer or oligomer assembly. The engineered disulfide bond between C2 and C282 is not anticipated to influence rhodopsin dimerization or oligomerization, unlike a scenario where a single cysteine is introduced into the opsin sequence. In that case, intermolecular disulfide bonds could form between different monomeric units, potentially altering the receptor oligomeric state. Additionally, the C2–C282 disulfide bond lies within the compact and highly structured intradiscal domain of the receptor (essential for correct opsin folding), which makes interactions with neighboring molecules unlikely.

The introduction of the engineered disulfide bond in G90$^{2.57}$Vs-s protein provides a structural counterbalance to the destabilizing effect of the naturally-occurring RP mutation, but its effects are fully reversed by DTT, which restores the native thermal stability profiles of both WTs-s and G90$^{2.57}$Vs-s. By reinforcing the connectivity between TM2 and TM7, this extra bridge helps to strengthen the stabilization effect of the N-terminal cap. This also extends to the retinal binding pocket, mitigating the negative effects of the G90$^{2.57}$V mutation on E113$^{3.28}$. This stabilization is evident in the improved capacity of the mutant to regenerate with 11CR and in the enhanced resistance to thermal and chemical denaturation, showing a potential role of this extra bond in the stabilization of all mutants, to some degree.

At a broader level, the disulfide bridge also supports the integrity of the ECLs and the terminal regions of the protein. The N-terminal region, essential for folding and trafficking, and the C-terminal region, involved in downstream signaling, both benefit from the improved stability of the core transmembrane structure. This global stabilization further underscores the potential of structural modifications or small molecule pharmaco-chaperones to rescue the function of destabilized GPCRs, such as Rho mutants associated with retinal diseases like RP. Although the engineered C2-C282 disulfide bond strongly enhances the conformational stability of the G90$^{2.57}$V mutant linked to RP, this biotechnological strategy faces practical challenges for clinical use. Along these lines, while the development of pharmaco-chaperones targeting native rhodopsin (without additional stabilizing disulfide bonds) is technically feasible and may promote protein stabilization, we believe that in highly thermally unstable mutants such as G90$^{2.57}$V, the stabilization achieved would always remain modest compared to that observed in our engineered variant.

CRediT authorship contribution statement

Pol Fernandez-Gonzalez: Writing – review & editing, Writing – original draft, Visualization, Validation, Methodology, Investigation, Formal analysis. **Sylwia Jencz:** Methodology, Investigation. **Steven O. Smith:** Writing – review & editing, Formal analysis. **Philip J. Reeves:** Writing – review & editing, Validation, Supervision, Formal analysis, Conceptualization. **Pere Garriga:** Writing – review & editing, Writing – original draft, Visualization, Validation, Supervision, Project administration, Funding acquisition, Formal analysis, Conceptualization.

Declaration of competing interest

The authors declare that they have no known competing financial interests or personal relationships that could have appeared to influence the work reported in this paper.

Acknowledgements

This research was funded by grants from Ministry of Science and Innovation, Spain (PID2019-104817GB-I00), and from the Government of Catalonia to Research Consolidated Groups (2021 SGR 00342) (P.G).

Data availability

Data will be made available on request.

References

[1] S.O. Smith, Mechanism of activation of the visual receptor rhodopsin, Annu. Rev. Biophys. 52 (2023) 301–317.
[2] A. Wu, et al., Structural basis for the allosteric modulation of rhodopsin by nanobody binding to its extracellular domain, Nature Communications 14 (1) (2023) 1–17.
[3] H. Nakamichi, T. Okada, X-ray crystallographic analysis of 9-cis-rhodopsin, a model analogue visual pigment†, Photochem. Photobiol. 83 (2007) 232–235.
[4] X.E. Zhou, K. Melcher, H.E. Xu, Structure and activation of rhodopsin, Acta Pharmacologica Sinica 33 (3) (2012) 291–299.
[5] J.A. Ballesteros, H. Weinstein, [19] Integrated methods for the construction of three-dimensional models and computational probing of structure-function relations in G protein-coupled receptors, Methods in Neurosciences 25 (1995) 366–428.
[6] M. Kono, P.W. Goletz, R.K. Crouch, 11-cis- and all-trans-retinols can activate rod opsin: rational design of the visual cycle, Biochemistry 47 (2008) 7567–7571.
[7] K. Rose, et al., Light regulation of rhodopsin distribution during outer segment renewal in murine rod photoreceptors, Curr. Biol. 34 (2024) 1492–1505.e6.
[8] D. Athanasiou, et al., The molecular and cellular basis of rhodopsin retinitis pigmentosa reveals potential strategies for therapy, Prog. Retin. Eye Res. 62 (2018) 1–23.
[9] P. Fernandez-Gonzalez, A. Mas-Sanchez, P. Garriga, Polyphenols and visual health: potential effects on degenerative retinal diseases, Molecules 26 (2021) 3407.
[10] S. Vasudevan, S. Senapati, M. Pendergast, P.S.-H. Park, Aggregation of rhodopsin mutants in mouse models of autosomal dominant retinitis pigmentosa, Nature Communications 15 (2024) 1–20.
[11] N. Cross, C. van Steen, Y. Zegaoui, A. Satherley, L. Angelillo, Retinitis Pigmentosa: burden of disease and current unmet needs, Clin. Ophthalmol. 16 (2022) 1993–2010.
[12] K.M. Malanson, J. Lem, Chapter 1 rhodopsin-mediated retinitis Pigmentosa, Prog. Mol. Biol. Transl. Sci. 88 (2009) 1–31.
[13] M.G. Herrera-Hernández, et al., Flavonoid allosteric modulation of mutated visual rhodopsin associated with retinitis pigmentosa, Scientific Reports 7 (1) (2017) 1–13.
[14] C.A. Opefi, K. South, C.A. Reynolds, S.O. Smith, P.J. Reeves, Retinitis pigmentosa mutants provide insight into the role of the N-terminal cap in rhodopsin folding, structure, and function, J. Biol. Chem. 288 (2013) 33912–33926.
[15] J. Standfuss, et al., Crystal structure of a thermally stable rhodopsin mutant, J. Mol. Biol. 372 (2007) 1179–1188.
[16] G. Xie, A.K. Gross, D.D. Oprian, An opsin mutant with increased thermal stability, Biochemistry 42 (2003) 1995–2001.
[17] D. Toledo, et al., Molecular mechanisms of disease for mutations at Gly-90 in rhodopsin, J. Biol. Chem. 286 (2011) 39993–40001.
[18] P.J. Reeves, J.M. Kim, H.G. Khorana, Structure and function in rhodopsin: a tetracycline-inducible system in stable mammalian cell lines for high-level expression of opsin mutants, Proc. Natl. Acad. Sci. U. S. A. 99 (2002) 13413–13418.
[19] F. Wang, P. Fernandez-Gonzalez, J.J. Perez, M. Morillo, P. Garriga, Retigabine increases the conformational stability of the visual photoreceptor rhodopsin, Int. J. Biol. Macromol. 279 (2024) 135343.
[20] T.D. Lamb, E.N. Pugh, Phototransduction, dark adaptation, and rhodopsin regeneration the proctor lecture, Invest. Ophthalmol. Vis. Sci. 47 (2006) 5138–5152.
[21] D. Deretic, et al., Rhodopsin C terminus, the site of mutations causing retinal disease, regulates trafficking by binding to ADP-ribosylation factor 4 (ARF4), Proc. Natl. Acad. Sci. U. S. A. 102 (2005) 3301–3306.
[22] C.F. Inglehearn, Molecular genetics of human retinal dystrophies, Eye (Basingstoke) 12 (1998) 571–579.
[23] C.T. Schafer, A. Shumate, D.L. Farrens, Novel fluorescent GPCR biosensor detects retinal equilibrium binding to opsin and active G protein and arrestin signaling conformations, J. Biol. Chem. 295 (2020) 17486–17496.
[24] G.F. Jang, et al., Mechanism of rhodopsin activation as examined with ring-constrained retinal analogs and the crystal structure of the ground state protein, J. Biol. Chem. 276 (2001) 26148–26153.

[25] Y. Gao, et al., Structures of the rhodopsin-Transducin complex: insights into G-protein activation, Mol. Cell 75 (2019) 781–790.e3.
[26] M. Zhang, et al., G protein-coupled receptors (GPCRs): advances in structures, mechanisms and drug discovery, Signal Transduction and Targeted Therapy 9 (2024) 1–43.
[27] D. Yang, et al., G protein-coupled receptors: structure- and function-based drug discovery, Signal Transduction and Targeted Therapy 6 (2021) 1–27.
[28] K. Alhosaini, A. Azhar, A. Alonazi, F. Al-Zoghaibi, GPCRs: the most promiscuous druggable receptor of the mankind, Saudi Pharmaceutical Journal 29 (2021) 539–551.
[29] K. Palczewski, et al., Crystal structure of rhodopsin: a G protein-coupled receptor, Science 1979 (289) (2000) 739–745.
[30] J. Liu, et al., Thermal properties of rhodopsin: insight into the molecular mechanism of dim-light vision, J. Biol. Chem. 286 (2011) 27622–27629.
[31] Y. Shichida, T. Morizumi, Mechanism of G-protein activation by rhodopsin†, Photochem. Photobiol. 83 (2007) 70–75.
[32] Y. Chinchore, A. Mitra, P.J. Dolph, Accumulation of rhodopsin in late endosomes triggers photoreceptor cell degeneration, PLoS Genet. 5 (2009).
[33] B.M. Tam, O.L. Moritz, The role of rhodopsin glycosylation in protein folding, trafficking, and light-sensitive retinal degeneration, J. Neurosci. 29 (2009) 15145.
[34] J. Hwa, J. Klein-Seetharaman, H.G. Khorana, Structure and function in rhodopsin: mass spectrometric identification of the abnormal intradiscal disulfide bond in misfolded retinitis pigmentosa mutants, Proc. Natl. Acad. Sci. U. S. A. 98 (2001) 4872–4876.
[35] E.C.Y. Yan, et al., Retinal counterion switch in the photoactivation of the G protein-coupled receptor rhodopsin, Proc. Natl. Acad. Sci. U. S. A. 100 (2003) 9262–9267.
[36] G. Khelashvili, et al., Unusual mode of dimerization of retinitis pigmentosa-associated F220C rhodopsin, Sci. Rep. 11 (2021) 1–20.
[37] T. Zhang, et al., Dimerization of visual pigments in vivo, Proc. Natl. Acad. Sci. U. S. A. 113 (2016) 9093–9098.